Formation temperatures of thermogenic and biogenic methane

D. A. Stolper *et al.*

Science **344**, 1500 (2014);
DOI: 10.1126/science.1254509

Science (print ISSN 0036-8075; online ISSN 1095-9203) is published weekly, except the last week in December, by the American Association for the Advancement of Science, 1200 New York Avenue NW, Washington, DC 20005.

slip length of 112 nm, implying that the velocity profile of the moving column is almost flat. Such a large slip length is supported by the strength of the interaction between liquid lead and the ZnO tube as well as by the nature of the experiment, which is carried out under far-from-equilibrium conditions.

The contact angles of liquid metals on metal oxide surfaces are usually larger than 90° (*26*, *27*); that is, the surface repels the liquid. For rough surfaces, such as the irregular inner walls of the ZnO tubes, this effect is even more pronounced. Under such nonwetting conditions, large slip lengths have been measured, up to tens of micrometers in the extreme case of superhydrophobic surfaces (*25*). We also note that the lead column may have an oxide skin (*28*), which increases the apparent viscosity of liquid metals at low shear rates (*27*). However, it is difficult to predict how this would affect the nanofluidic behavior at the high shear rates in our experiment (~10^7 s^{-1}, as estimated from the flow velocity and the tube dimensions). Under such conditions, the slip length may also increase with shear rate. Simulations for smooth surfaces have found the slip length to diverge at shear rates of ~10^8 s^{-1} (*25*, *29*). Moreover, on rough surfaces, large shear rate–dependent slip lengths have been demonstrated experimentally (*30*); however, nano-sized vapor bubbles on the surface may play a role in such experiments (*30*).

We believe that the approach presented here should find applications in the study of nanoscale phenomena that have previously been inaccessible, including the investigation of nanofluidic structures or biological channels (*31*) with high spatial and temporal resolutions. The study of phase transitions in nanoconfined environments constitutes another area that will benefit from the capability to manipulate and visualize single nanotubes in situ.

REFERENCES AND NOTES

1. J. C. T. Eijkel, A. van den Berg, *Microfluid. Nanofluid.* **1**, 249–267 (2005).
2. L. Bocquet, E. Charlaix, *Chem. Soc. Rev.* **39**, 1073–1095 (2010).
3. M. Majumder, N. Chopra, R. Andrews, B. J. Hinds, *Nature* **438**, 44 (2005).
4. J. K. Holt *et al.*, *Science* **312**, 1034–1037 (2006).
5. M. Whitby, L. Cagnon, M. Thanou, N. Quirke, *Nano Lett.* **8**, 2632–2637 (2008).
6. M. Whitby, N. Quirke, in *Handbook of Nanophysics: Nanotubes and Nanowires*, K. D. Sattler, Ed. (CRC Press, Boca Raton, FL, 2011), chap. 11.
7. J. M. Yuk *et al.*, *Science* **336**, 61–64 (2012).
8. Q. Chen *et al.*, *Nano Lett.* **13**, 4556–4561 (2013).
9. N. Naguib *et al.*, *Nano Lett.* **4**, 2237–2243 (2004).
10. J. Y. Chen, A. Kutana, C. P. Collier, K. P. Giapis, *Science* **310**, 1480–1483 (2005).
11. Y. Gogotsi, J. A. Libera, A. Guvenc-Yazicioglu, C. M. Megaridis, *Appl. Phys. Lett.* **79**, 1021–1023 (2001).
12. M. P. Rossi *et al.*, *Nano Lett.* **4**, 989–993 (2004).
13. A. Siria *et al.*, *Nature* **494**, 455–458 (2013).
14. A. H. Zewail, *Science* **328**, 187–193 (2010).
15. A. H. Zewail, J. M. Thomas, *4D Electron Microscopy: Imaging in Space and Time* (Imperial College Press, London, 2010).
16. See supplementary materials on *Science* Online.
17. C.-Y. Wang, N.-W. Gong, L.-J. Chen, *Adv. Mater.* **20**, 4789–4792 (2008).
18. P. J. Linstrom, W. G. Mallard, Eds., *Thermodynamics Source Database* (NIST Chemistry WebBook, NIST Standard Reference Database No. 69; National Institute of Standards and Technology, Gaithersburg, MD, 2014).
19. S. Link, C. Burda, B. Nikoobakht, M. A. El-Sayed, . *Chem. Phys. Lett.* **315**, 12–18 (1999).
20. C. Y. Ruan, Y. Murooka, R. K. Raman, R. A. Murdick, *Nano Lett.* **7**, 1290–1296 (2007).
21. H. Sakai, *Surf. Sci.* **351**, 285–291 (1996).
22. P.-G. de Gennes, F. Brochard-Wyart, D. Quere, *Capillarity and Wetting Phenomena: Drops, Bubbles, Pearls, Waves* (Springer, New York, 2004).
23. Similar values for f were obtained when x_e was varied. We determined f_0 to be 2.14×10^{-2} Pa·s using the viscosity of bulk lead at 1700 K, the estimated temperature of the tube after the laser pulse (*16*); shear thinning is expected to be insignificant despite the high shear rate in our experiment (*32*). For other nanotubes of larger diameter, on the order of 100 nm, similar friction coefficients were obtained.
24. M. Whitby, N. Quirke, *Nat. Nanotechnol.* **2**, 87–94 (2007).
25. L. Bocquet, J. L. Barrat, *Soft Matter* **3**, 685–693 (2007).
26. D. Chatain, *Annu. Rev. Mater. Res.* **38**, 45–70 (2008).
27. Q. Xu, N. Oudalov, Q. T. Guo, H. M. Jaeger, E. Brown, *Phys. Fluids* **24**, 063101 (2012).
28. G. Yi, W. Schwarzacher, *Appl. Phys. Lett.* **74**, 1746–1748 (1999).
29. P. A. Thompson, S. M. Troian, *Nature* **389**, 360–362 (1997).
30. C. Cottin-Bizonne, B. Cross, A. Steinberger, E. Charlaix, *Phys. Rev. Lett.* **94**, 056102 (2005).
31. E. Tajkhorshid *et al.*, *Science* **296**, 525–530 (2002).
32. C. Desgranges, J. Delhommelle, *Phys. Rev. B* **78**, 184202 (2008).
33. *Handbook on Lead-Bismuth Eutectic Alloy and Lead Properties, Materials Compatibility, Thermal-Hydraulics and Technologies* (Nuclear Energy Agency, Organisation for Economic Co-operation and Development, 2007).

ACKNOWLEDGMENTS

Supported by NSF grant DMR-0964886 and Air Force Office of Scientific Research grant FA9550-11-1-0055 in the Physical Biology Center for Ultrafast Science and Technology at Caltech, which is supported by the Gordon and Betty Moore Foundation. U.J.L. was partly supported by a postdoctoral fellowship from the Swiss National Science Foundation.

SUPPLEMENTARY MATERIALS

www.sciencemag.org/content/344/6191/1496/suppl/DC1
Materials and Methods
Supplementary Text
Figs. S1 to S6
Movies S1 and S2
References (*34*–*40*)

19 March 2014; accepted 27 May 2014
10.1126/science.1253618

GAS FORMATION

Formation temperatures of thermogenic and biogenic methane

D. A. Stolper,[1]* M. Lawson,[2] C. L. Davis,[2] A. A. Ferreira,[3] E. V. Santos Neto,[3] G. S. Ellis,[4] M. D. Lewan,[4] A. M. Martini,[5] Y. Tang,[6] M. Schoell,[7] A. L. Sessions,[1] J. M. Eiler[1]

Methane is an important greenhouse gas and energy resource generated dominantly by methanogens at low temperatures and through the breakdown of organic molecules at high temperatures. However, methane-formation temperatures in nature are often poorly constrained. We measured formation temperatures of thermogenic and biogenic methane using a "clumped isotope" technique. Thermogenic gases yield formation temperatures between 157° and 221°C, within the nominal gas window, and biogenic gases yield formation temperatures consistent with their comparatively lower-temperature formational environments (<50°C). In systems where gases have migrated and other proxies for gas-generation temperature yield ambiguous results, methane clumped-isotope temperatures distinguish among and allow for independent tests of possible gas-formation models.

The environmental conditions, rates, and mechanisms of methane formation are critical to understanding the carbon cycle and for predicting where economically substantial amounts of methane form. Conventional models of thermogenic methane formation predict that (i) gas formation is kinetically controlled by time, temperature, and organic matter composition (*1*); (ii) gases cogenerated with oil form below ~150° to 160°C (*2*–*4*); and (iii) gases created from the breakdown (cracking) of oil or refractory kerogen form above ~150° to 160°C (*2*–*4*). Microbially produced (biogenic) methane in nature is thought to form mostly below ~80°C (*5*, *6*).

Our understanding of the kinetics of thermogenic methane formation is dominantly constrained by extrapolating kinetic parameters from high-temperature (~>300°C) laboratory experiments to lower-temperature (~100° to 200°C), geologically relevant conditions (*7*). These experiments are sensitive to heating rates (*7*) and the activity of water (*1*, *7*–*10*), minerals (*1*), and transition metals (*11*); the observed range of derived kinetic parameters can result in divergent predictions for natural methane-formation temperatures (*1*, *10*). Additionally, many thermogenic gases have migrated from their source to a reservoir (*3*, *12*–*14*). Although these migrated gases dominate the data sets used to calibrate empirical models of thermogenic methane formation

[1]Division of Geological and Planetary Sciences, California Institute of Technology, 1200 East California Boulevard, Pasadena, CA 91125, USA. [2]ExxonMobil Upstream Research Company, Houston, TX, USA. [3]Division of Geochemistry, Petrobras Research and Development Center (CENPES), Rio de Janeiro, RJ, Brazil. [4]U.S. Geological Survey, Denver Federal Center, Denver, CO, USA. [5]Department of Geology, Amherst College, Amherst, MA, USA. [6]Power, Environmental, and Energy Research Institute, Covina, CA, USA. [7]GasConsult International Inc, Berkeley, CA, USA.
***Corresponding author. E-mail: dstolper@caltech.edu**

(*3*, *13*–*15*), the ability to understand their thermal histories, and thus accurately calibrate models, is hampered by (i) a lack of independent constraints on the thermal histories of the source and reservoir rocks and the timing of gas migration, and (ii) the possibility that a reservoir contains a mixture of gases from different sources. Finally, biogenic gases are produced ubiquitously in near-surface sedimentary environments (*6*, *16*) and can comingle with thermogenic gases (*17*). Despite the many empirical tools used to distinguish biogenic from thermogenic gases (*18*), identifying the sources and quantifying relative contributions of biogenic and thermogenic gases in nature remains challenging (*17*).

We measured multiply substituted ("clumped") isotope temperatures of methane (*19*) generated via the experimental pyrolysis of larger organic molecules and sampled from natural thermogenic deposits of the Haynesville Shale (USA), Marcellus Shale (USA), and Potiguar Basin (Brazil) (*20*) and from natural systems with methanogens from the Gulf of Mexico and Antrim Shale (USA). We quantified the abundance of both $^{13}CH_3D$ and $^{12}CH_2D_2$, two clumped isotopologues of methane, relative to a random isotopic distribution via the parameter Δ_{18} (*20*). For isotopically equilibrated systems, Δ_{18} values are a function of temperature, dependent only on the isotopic composition of methane, and thus can be used to calculate methane-formation temperatures (Fig. 1A) (*19*, *20*, *21*). It was not obvious before this work what Δ_{18}-based temperatures of natural samples would mean, in part because conventional models assume that methane forms via kinetically (as opposed to equilibrium) controlled reactions (*1*–*3*, *8*, *22*–*24*).

We generated methane from larger hydrocarbon molecules at constant temperatures in two experiments: pyrolysis of propane at 600°C (*20*) and closed-system hydrous pyrolysis (*7*, *9*) of organic matter at 360°C (*20*). For both, Δ_{18} temperatures are within 2 standard deviations (σ) of experimental temperatures (Fig. 1A and table S1). This supports the suggestion in (*19*) that measured Δ_{18}-based temperatures of thermogenic methane could record formation temperatures.

We next examined thermogenic shale gases from the Haynesville Shale (*25*). In shale-gas systems, the shale is both the source and reservoir for generated hydrocarbons (*26*), thus minimizing complications associated with gas migration for our interpretations. Geological constraints indicate that the Haynesville Shale has undergone minimal uplift (~<0.5 km) (20) since reaching maximum burial temperatures (modeled to currently be within 5° to 17°C of maximum burial temperatures; tables S2 and S3) (20). Measured Δ_{18} temperatures range from 169° to 207°C, overlapping, within uncertainty, current reservoir temperatures (163° to 190°C; Fig. 1, A and B, and table S2). We also compared the Δ_{18} temperatures to independently calculated gas-formation temperatures using the generation kinetics of Burnham (*20*, *27*). Modeled average gas-formation temperatures from secondary oil breakdown range from 168° to 175°C (table S3) (20). The modeled temperatures are lower than, but within uncertainty of, measured Δ_{18} temperatures (table S2). This difference likely reflects the fact that the model calculates an average formation temperature that includes all hydrocarbon gases (i.e., $C_{1\text{-}5}$ alkanes), but the types of experiments used to calibrate the model generate methane at a higher average temperature than other hydrocarbon gases (*28*). Thus, average methane-formation temperatures should be higher than those modeled for average hydrocarbon gas-formation temperatures. Consequently, Δ_{18} temperatures are consistent with expected methane-formation temperatures. However, in this case, it is also possible that methane reequilibrated from some other, initial Δ_{18} value to one consistent with its subsequent storage temperatures.

Next, we considered shale gases from uplifted rocks (>3 km of uplift after maximum burial) (20) in the Marcellus Shale (*29*), which reached modeled maximum burial temperatures of 183° to 219°C, but today are 60° to 70°C (tables S2 and S3) (20). This system allows us to examine the effects of gradual cooling and long-term storage at temperatures colder than methane-formation temperatures on Δ_{18} values. Samples yield Δ_{18} temperatures from 179° to 207°C, overlapping those for the Haynesville Shale and hotter than current reservoir temperatures (Fig. 1B). Modeled formation temperatures (using the Burnham kinetics as above) (27) are 171° to 173°C (table S3)—the modeled temperatures are again slightly lower than the measured Δ_{18} temperatures (for reasons discussed above), but the two are within analytical uncertainty (table S2). We conclude that Δ_{18} temperatures of Marcellus Shale methane are indistinguishable from independent expectations regarding methane-formation temperatures and were not noticeably influenced by later cooling.

We also examined thermogenic gases from the southwestern sector of the Potiguar Basin (*30*) that migrated from deeper sources to shallower reservoirs (*31*). Here, measured Δ_{18} temperatures range from 157° to 221°C and exceed current reservoir temperatures (66° to 106°C; table S2). This is consistent with vertical migration of gases from hotter sources to cooler reservoirs (*3*). We note that some source rocks in the Potiguar Basin near where samples were collected have experienced sufficient burial temperatures to reach a vitrinite reflectance of 2.7%, within the range observed for the Haynes ville and Marcellus Shale gas source rocks (1.7 to 3.1%; table S3) and consistent with the high-temperature (>150° to 160°C) (2–4)

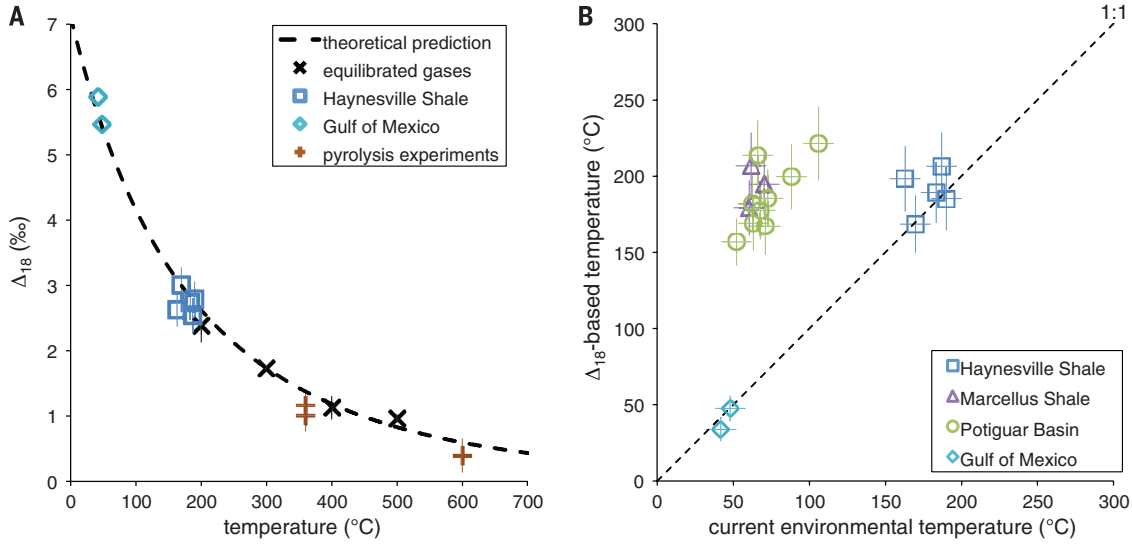

Fig. 1. Comparisons of Δ_{18} temperatures to environmental/formation temperatures. (**A**) Formation/reservoir temperatures versus Δ_{18} values. The dashed line is the theoretical dependence of Δ_{18} on temperature (*19*). Equilibrated gas data are from (*19*). Temperatures are formation/equilibration temperatures for the pyrolysis and equilibrated samples and current reservoir temperatures for the Haynesville Shale and Gulf of Mexico samples. (**B**) Current reservoir temperatures versus Δ_{18} temperatures for all natural samples investigated except the Antrim Shale samples, which are excluded because they are a mixture of thermogenic and biogenic gases. The dotted line is a 1:1 line. Uncertainty for well temperatures is estimated to be ~±10°C. Error bars are 1σ.

"dry gas zone" in which oil is hypothesized to crack to gas (*3*). Thus, the Δ_{18} temperatures from Potiguar Basin methane (157° to 221°C) are compatible with the thermal history of some source rocks in the region. Additionally, a positive correlation exists between the Δ_{18} temperatures and $\delta^{13}C$ values (*32*) of Potiguar Basin gases (Fig. 2; $P = 0.008$) with a slope, 5.3°C/per mil (‰) (±2.2; 1σ), within error of some theoretical estimates, 8.8°C/‰ (*20*, *22*) and 9.4°C/‰ (*20*, *23*). This relationship is expected because earlier-generated methane is thought to form at lower temperatures with lower $\delta^{13}C$ values than methane formed later at higher temperatures (*2*, *3*, *15*, *23*). The Potiguar Basin samples raise the issue that mixing of gases with differing $\delta^{13}C$ and δD values can result in Δ_{18} values that are not simply weighted averages of the endmembers (*19*, *20*). However, in this specific case (and for the shale gases), $\delta^{13}C$ and δD values do not span a sufficiently large range for mixing between samples to result in Δ_{18}-based temperatures different (within analytical uncertainty) from the actual average formation temperatures of the mixtures (fig. S2) (20).

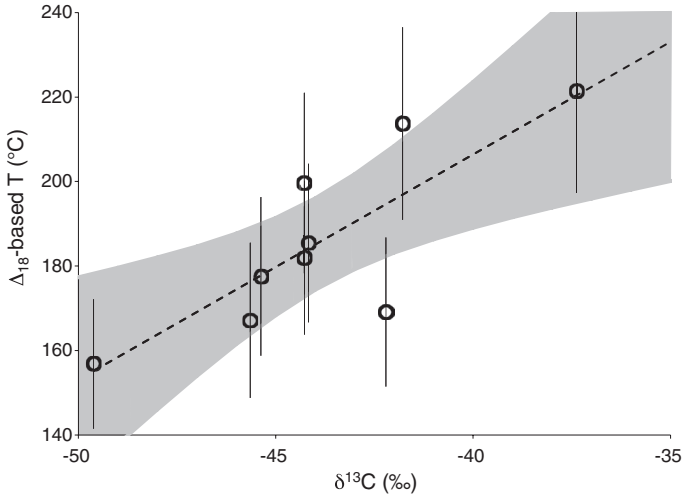

Fig. 2. $\delta^{13}C$ values versus Δ_{18} temperatures for methane from the Potiguar Basin. A positive correlation ($P = 0.008$) between $\delta^{13}C$ values and Δ_{18}-based temperatures of methane is observed. The gray band is the 95% confidence interval for the linear regression through the data. Error bars are 1σ.

The data discussed above are consistent with the interpretation that Δ_{18} values of thermogenic methane reflect isotopic equilibrium at the temperature of methane formation and that the "closure temperature" above which Δ_{18} values can freely re-equilibrate is ~>200°C in geological environments because (i) experimentally generated methane yields Δ_{18} values within error of formation temperatures (Fig. 1A). (ii) All Δ_{18} temperatures from natural samples are geologically reasonable formation temperatures (*1*–*4*, *10*). (iii) Haynesville Shale Δ_{18} temperatures are within uncertainty of current and modeled maximum burial temperatures (Fig. 1, A and B). (iv) Haynesville and Marcellus Shale Δ_{18} temperatures are within error of independently modeled gas-formation temperatures. (v) Haynesville and Marcellus Shale Δ_{18} temperatures overlap despite the differing thermal histories of each system (the Marcellus Shale cooled by >100°C after gas generation). This would not be expected if Δ_{18} temperatures represent closure temperatures and thus reset during cooling of the host rocks. And (vi) Potiguar Basin Δ_{18} temperatures and $\delta^{13}C$ values are positively correlated (Fig. 2), with a slope within error of theoretical predictions.

The agreement between the Haynesville and Marcellus Shale methane Δ_{18} temperatures and

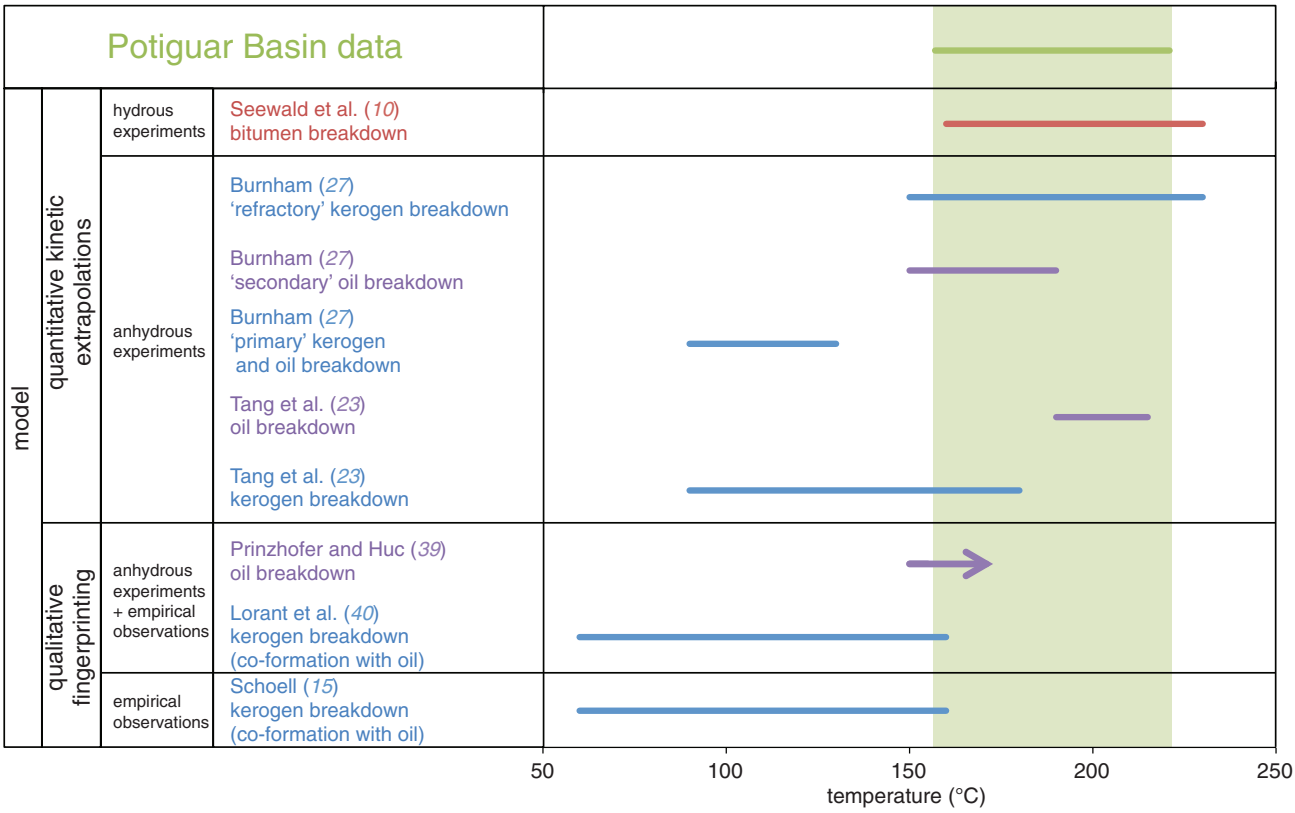

Fig. 3. Comparison of modeled methane-formation temperatures to Δ_{18} temperatures. Blue lines indicate gases generated from kerogen breakdown; purple lines, gases generated from oil breakdown; and red line, gases generated from bitumen breakdown. The green line indicates the measured range of Δ_{18} temperatures from the Potiguar Basin. Models are from (*10*, *15*, *23*, *27*, *39*, *40*) and described in (*20*).

modeled formation temperatures demonstrates that relatively simple gas-generation models are accurate when the thermal histories of the source rocks are constrained. The formation temperatures of the Potiguar Basin gases are challenging to constrain with such models due to gas migration, which obscures the location and timing of gas formation. Previously, these gases were interpreted to have been cogenerated with oils (*30*) and thus below ~160°C (*2*–*4*). This disagreement between our data and published interpretations inspired us to examine a range of gas-formation models (*20*) for the Potiguar Basin samples (Fig. 3). All models presented are in common use and constrained by similar gas chemistry data (*20*); however, many disagree with each other and together predict a range of >170°C for gas formation (Fig. 3). The Δ_{18} temperatures allow these models to be independently evaluated, rejecting some (e.g., low-temperature gas generation solely from kerogen) and narrowing the permitted interpretations. Specifically, methane in the Potiguar Basin could have formed via the mixing of gases produced by low-temperature (~<150° to 180°C) kerogen breakdown with gases generated from higher-temperature (~>150° to 160°C) oil breakdown, consistent with the models of Tang *et al*. (*23*) and Burnham (*27*). This scenario requires a specific set of mixing components to generate the observed formation temperatures, $C_1/\Sigma C_{1\text{-}5}$ values (table S2), and correlation between Δ_{18} temperatures and methane $\delta^{13}C$ values. Alternatively, the model of Seewald *et al*. (*10*), which is the only model presented to incorporate the importance of water in gas formation, is consistent with the Δ_{18} temperatures and $C_1/\Sigma C_{1\text{-}5}$ values (<85%; table S2) for the Potiguar Basin gases. This may indicate that water should be considered in models of methane formation. Although the gas-generation temperatures derived from the breakdown of refractory kerogen, as in the model of Burnham (*27*), appear compatible with the Δ_{18} temperatures (Fig. 3), this organic source dominantly generates methane (*27*) and thus cannot be the sole source of gas to the system due to the high concentration of $C_{2\text{-}5}$ alkanes in the gases (<85% $C_1/\Sigma C_{1\text{-}5}$; table S2).

Thus, while the addition of Δ_{18} temperatures does not provide a unique interpretation of the origin of the Potiguar Basin gases, it rules out several otherwise plausible interpretations and places specific constraints on the remaining models. Notably, our results for the Potiguar Basin indicate that the formation environments for methane extend to higher temperatures (and presumably depths) in this system than many models of petroleum genesis predicted (Fig. 3) and supports experimental evidence that substantial quantities of methane can be generated at higher temperatures than is sometimes appreciated (*33*). This observation requires that this basin possesses a previously unsuspected "root" that reached high temperatures at some point in its history, generating high-temperature methane that ascended into shallower reservoirs. Thus, Δ_{18} temperatures not only constrain the conditions and mechanisms of methane formation, but also provide a window into the geological and thermal histories of basins in which methane forms.

To examine Δ_{18}-based temperatures from known low-temperature sources of methane, we measured Δ_{18} values from two sources of biogenic gases produced from the biodegradation of oil (Gulf of Mexico). They return Δ_{18} temperatures (34° ± 8°C and 48° ± 8°C) within error of their current reservoir temperatures (42° and 48°C, respectively; Fig. 1, A and B, and table S2). We further measured two gases from the Antrim Shale, which has been interpreted as containing a mixture of biogenic gases higher in $C_1/\Sigma C_{1\text{-}5}$ and thermogenic gases lower in $C_1/\Sigma C_{1\text{-}5}$ (*17*). The sample closer to the biogenic endmember (99.99% $C_1/\Sigma C_{1\text{-}5}$) returns a Δ_{18} temperature of 40°C (±10; 1σ), whereas the sample interpreted here to be closer to a thermogenic endmember (88.9% $C_1/\Sigma C_{1\text{-}5}$) returns a higher temperature of 115°C (±12°C; 1σ). Thus, the natural biogenic gases have Δ_{18} temperatures consistent with their expected formation temperatures, both as pure endmembers and as dominant components of mixtures. We note that preliminary results for methanogens grown in pure culture (*34*) indicate that they can produce methane out of internal isotopic equilibrium. Nevertheless, our measurements of natural biogenic methane indicate that natural environments (at least those investigated to date) permit the attainment of local internal isotopic equilibrium in methane.

These results indicate that Δ_{18} values can be used to calculate formation temperatures of methane from both pure and mixed thermogenic and biogenic gas deposits and interrogate models of gas formation and geological histories of basins. Additionally, if the interpretation of Δ_{18}-based temperatures as formation temperatures is correct, it has implications for our understanding of the chemistry of thermogenic and biogenic methane formation. Specifically, it requires a previously unrecognized step for both processes that allows C-H bonds to equilibrate during methane formation. This interpretation is unexpected because $\delta^{13}C$ values of thermogenic and biogenic methane are almost universally considered to be controlled by kinetic-isotope effects rather than equilibrium-thermodynamic effects (*2*, *16*, *22*–*24*, *35*). This apparent contradiction can be reconciled if reacting methane precursors (e.g., methyl groups) undergo local hydrogen exchange faster than the rate of net methane generation. For thermogenic gases, this could occur via exchange reactions with water (*36*) or catalytic hydrogen exchange on organic macromolecules, mineral surfaces, or transition metals (*11*, *37*). For biogenic methane, reversible hydrogen exchange could occur on methane or methane precursors if the pathway for methane formation is partially reversible (*35*, *38*). Thus, Δ_{18} measurements may also elucidate chemical and biochemical mechanisms of methane formation.

REFERENCES AND NOTES

1. J. S. Seewald, *Nature* **426**, 327–333 (2003).
2. C. Clayton, *Mar. Pet. Geol.* **8**, 232–240 (1991).
3. J. M. Hunt, *Petroleum Geochemistry and Geology* (Freeman, New York, 1996).
4. T. Quigley, A. Mackenzie, *Nature* **333**, 549–552 (1988).
5. A. Wilhelms *et al*., *Nature* **411**, 1034–1037 (2001).
6. D. L. Valentine, *Annu. Rev. Mar. Sci.* **3**, 147–171 (2011).
7. M. Lewan, T. Ruble, *Org. Geochem.* **33**, 1457–1475 (2002).
8. J. Espitalié, P. Ungerer, I. Irwin, F. Marquis, *Org. Geochem.* **13**, 893–899 (1988).
9. M. Lewan, *Geochim. Cosmochim. Acta* **61**, 3691–3723 (1997).
10. J. S. Seewald, B. C. Benitez-Nelson, J. K. Whelan, *Geochim. Cosmochim. Acta* **62**, 1599–1617 (1998).
11. F. D. Mango, J. Hightower, *Geochim. Cosmochim. Acta* **61**, 5347–5350 (1997).
12. W. England, A. Mackenzie, D. Mann, T. Quigley, *J. Geol. Soc. London* **144**, 327–347 (1987).
13. L. C. Price, M. Schoell, *Nature* **378**, 368–371 (1995).
14. B. P. Tissot, D. H. Welte, *Petroleum Formation and Occurrence: A New Approach to Oil and Gas Exploration* (Springer-Verlag, Berlin, 1978).
15. M. Schoell, *AAPG Bull.* **67**, 2225 (1983).
16. M. J. Whiticar, E. Faber, M. Schoell, *Geochim. Cosmochim. Acta* **50**, 693–709 (1986).
17. A. M. Martini, J. M. Budai, L. M. Walter, M. Schoell, *Nature* **383**, 155–158 (1996).
18. M. J. Whiticar, *Chem. Geol.* **161**, 291–314 (1999).
19. D. A. Stolper *et al*., *Geochim. Cosmochim. Acta* **126**, 169–191 (2014).
20. Materials and methods are available as supplementary materials on *Science* Online.
21. J. M. Eiler, *Earth Planet. Sci. Lett.* **262**, 309–327 (2007).
22. Y. Ni *et al*., *Geochim. Cosmochim. Acta* **75**, 2696–2707 (2011).
23. Y. Tang, J. Perry, P. Jenden, M. Schoell, *Geochim. Cosmochim. Acta* **64**, 2673–2687 (2000).
24. Y. Xiao, *Rev. Mineral. Geochem.* **42**, 383–436 (2001).
25. U. Hammes, H. S. Hamlin, T. E. Ewing, *AAPG Bull.* **95**, 1643–1666 (2011).
26. J. B. Curtis, *AAPG Bull.* **86**, 1921 (2002).
27. A. Burnham, "A simple kinetic model of petroleum formation and cracking" (Lawrence Livermore National Lab, report UCID 21665, 1989).
28. P. Ungerer, *Org. Geochem.* **16**, 1–25 (1990).
29. G. G. Lash, T. Engelder, *AAPG Bull.* **95**, 61–103 (2011).
30. A. Prinzhofer, E. V. Dos Santos Neto, A. Battani, *Mar. Pet. Geol.* **27**, 1273–1284 (2010).
31. L. Trindade, S. C. Brassell, E. V. Santos Neto, *AAPG Bull.* **76**, 1903 (1992).
32. $\delta = (R/R_{std} - 1) \times 1000$ where $^{13}R = [^{13}C]/[^{12}C]$, $^{D}R = [D]/[H]$, and "std" denotes the standard to which all measurements are referenced (Vienna Pee Dee belemnite for carbon and Vienna standard mean ocean water for hydrogen isotopes).
33. N. Mahlstedt, B. Horsfield, *Mar. Pet. Geol.* **31**, 27–42 (2012).
34. D. A. Stolper *et al*., *Mineral. Mag.* **78**, 2393 (2014).
35. D. L. Valentine, A. Chidthaisong, A. Rice, W. S. Reeburgh, S. C. Tyler, *Geochim. Cosmochim. Acta* **68**, 1571–1590 (2004).
36. T. Hoering, *Org. Geochem.* **5**, 267–278 (1984).
37. F. D. Mango, J. Hightower, A. T. James, *Nature* **368**, 536–538 (1994).
38. S. Scheller, M. Goenrich, R. Boecher, R. K. Thauer, B. Jaun, *Nature* **465**, 606–608 (2010).
39. A. A. Prinzhofer, A. Y. Huc, *Chem. Geol.* **126**, 281–290 (1995).
40. F. Lorant, A. Prinzhofer, F. Behar, A.-Y. Huc, *Chem. Geol.* **147**, 249–264 (1998).

ACKNOWLEDGMENTS

This work was supported by the NSF, Petrobras, ExxonMobil, and Caltech. We thank Petrobras and ExxonMobil for providing samples and permission to publish, C. Araújo and B. Peterson for helpful discussions, and R. Burruss and three anonymous reviewers for helpful comments on the manuscript. Any use of trade, firm, or product names is for descriptive purposes only and does not imply endorsement by the U.S. Government. All data used to support the conclusions in this manuscript are provided in the supplementary materials.

SUPPLEMENTARY MATERIALS

www.sciencemag.org/content/344/6191/1500/suppl/DC1
Materials and Methods
Supplementary Text
Figs. S1 to S5
Tables S1 to S6
References (*41*–*63*)

8 April 2014; accepted 2 June 2014
10.1126/science.1254509